AGU PUBLICATIONS

Journal of Advances in Modeling Earth Systems

RESEARCH ARTICLE

10.1002/2014MS000318

Key Points:
- Vertical velocities for different plume types are parameterized
- Momentum sources and sinks are analyzed for different plume types
- Differences between convective core, updraft, and clouds are presented

Correspondence to:
M. Zhang,
minghua.zhang@stonybrook.edu

Citation:
Wang, X., and M. Zhang (2014), Vertical velocity in shallow convection for different plume types, *J. Adv. Model. Earth Syst.*, *6*, 478–489, doi:10.1002/2014MS000318.

Received 7 MAR 2014
Accepted 8 MAY 2014
Accepted article online 14 MAY 2014
Published online 10 JUN 2014

Vertical velocity in shallow convection for different plume types

Xiaocong Wang[1,2] and Minghua Zhang[2]

[1]State Key Laboratory of Numerical Modeling for Atmospheric Sciences and Geophysical Fluid Dynamics, Institute of Atmospheric Physics, Chinese Academy of Sciences, Beijing, China, [2]School of Marine and Atmospheric Sciences, Stony Brook University, Stony Brook, New York, USA

Abstract This study investigates the bulk budgets of the vertical velocity and its parameterization in convective cores, convective updrafts, and clouds by using large-eddy simulation (LES) of four shallow convection cases in the Global Energy and Water Cycle Experiment (GEWEX) Cloud System Study (GCSS) programs. The relative magnitudes of the dominant momentum budget terms for the three types of plumes are presented. For all shallow cumulus except stratocumulus, the buoyancy force and the subplume transport in the core plume are the momentum source that offset the pressure gradient force. In the cloud updraft and cloud plumes, the buoyancy source is dominant in the lower and middle parts of the clouds, while the subgrid transport is a dominant source in the upper part, and the entrainment term is also a momentum source. For the stratocumulus, the subplume transport is a sink almost in the whole convective layer. For all types of plumes, the Simpson and Wiggert (1969) equation is found to be good paramaterization of the mean plume vertical velocity when appropriate scaling coefficients to buoyancy and entrainment terms are used. Optimal forms of the Simpson and Wiggert equation are given for convective cores, convective updrafts, and convective clouds. Results are compared with other studies published in the literature.

1. Introduction

The parameterization of air vertical velocity within cumulus clouds in large-scale models has been a subject of active research [e.g., *Gregory*, 2001; *Wu et al*., 2009; *Del Genio and Wu*, 2010]. The mean vertical velocity in convective clouds is desired for several reasons. For example, it is needed to determine the cloud top height. Traditionally, the neutral buoyancy level (NBL) is defined as the cloud top in most early convection schemes [e.g., *Arakawa and Schubert*, 1974; *Tiedtke*, 1989; *Zhang and McFarlane*, 1995]. However, the actual cloud top is typically higher than the NBL, since the cloud parcel can still travel some distance before its velocity completely vanishes, creating the so-called overshooting region [*Wyant et al*., 1997]. To parameterize overshooting of cumulus convection, it is necessary to introduce the in-cloud vertical velocity equation. Furthermore, vertical velocity is needed to calculate cloud nucleation and the falling velocity of precipitation [e.g., *Peng et al*., 2005; *Fountoukis et al*., 2007]. Additionally, many shallow convection schemes calculate the mass fluxes of the plumes. Thus, when the vertical velocity is known for an entraining plume, the fractional area of the plume can be derived.

Most convection schemes employ the *Simpson and Wiggert* [1969] equation to calculate the mean in-cloud vertical velocity, w_c, which is jointly controlled by the buoyancy force, B_c, and the drag effect caused by entrainment rate, ε, written as

$$w_c \frac{\partial w_c}{\partial z} = aB_c - b\varepsilon w_c^2, \tag{1}$$

where z stands for height, coefficients a and b are empirical constants. Different studies used different values of a and b. For example, *Soares et al*. [2004] used $a=2$ and $b=1$ in their parameterization scheme, while *Bretherton et al*. [2004] used $a=1$ and $b=2$ in their shallow convection scheme. The second and third columns of Table 1 list values of a and b used in previous studies.

One source of the difference is the precise definition of the plume in shallow convection. Some studies defined it as the fraction of positively buoyant upward fraction of air that contains condensed water, which

Table 1. Coefficients *a* and *b* Used in the Literature and From This Study

Reference	*a*	*b*
Bechtold et al. [2001]	2/3	1
Bretherton et al. [2004]	1	2
Cheinet [2004]	1	1
de Rooy and Siebesma [2010]	0.62	1
ECMWF [2010]	1/3	1.95
Jakob and Siebesma [2003]	1/3	2
Neggers et al. [2009]	10/7	5/7
Pergaud et al. [2009]	1	1
Soares et al. [2004]	2	1
Core	0.40	1.06
Updraft	0.19	−0.29
Cloud	0.14	−0.02

is referred to as convective core. Others defined it as upward fraction of air that contains condensed water without the positive buoyancy condition, referred to as updraft. In almost all schemes, the cloud fraction is considered to be the same as the plume, even though cloud area may be negatively buoyant and in downward motion.

The purpose of this paper is to evaluate the vertical momentum budget and to derive parameterizations of the mean velocity separately for the three types of plumes—convective core, convective updraft, and cloud plume. Most current parameterization schemes of shallow convection only use one plume type in which fractional area of a plume is assumed to be the same as the cloud amount. However, more than one plume type may be needed to describe different roles of cumulus convection. For example, convective core is more relevant to cloud nucleation, while convective updraft is more relevant to condensation, and cloud plume is more relevant to radiation. The present study addresses the parameterization of vertical velocity in the different plume types.

This paper is divided into the following sections: section 2 introduces the LES model and four shallow convection cases. Section 3 investigates the budget terms for the full vertical velocity equation of the three types of plumes. Also explored in this section are the diagnostics of entrainment rate. Section 4 is about the parameterization of in-cloud vertical velocity and its comparison with previous studies. Finally, the last section gives a summary.

2. LES Case Descriptions and Simulations

2.1. Case Descriptions

Four shallow convection cases are chosen in this study, which come from the Global Energy and Water Cycle Experiment (GEWEX) Cloud System Studies (GCSS) Working Group on boundary layer clouds, including three marine equilibrium trade wind cases and one transient continental cumulus case. They are the Barbados Oceanographic and Meteorological Experiment (BOMEX) [*Siebesma et al.*, 2003], Rain in Cumulus over the Ocean (RICO) [*Vanzanten et al.*, 2011], the Atlantic Trade Wind Experiment (ATEX) [*Stevens et al.*, 2001], and the Atmospheric Radiation Measurement Program-Southern Great Plains site (ARM-SGP) case study of continental shallow convection [*Brown et al.*, 2002]. The three maritime convection cases are different in the inversion strength, while ARM-SGP gives a nonsteady continent convection case. As a result, these four cases span a range of shallow cumulus and stratocumulus regimes that occur in low and middle latitudes.

2.2. Model and Experiments

The LES model used in this study is SAM (System for Atmospheric Modeling), which was kindly provided by Marat Khairoutdinov of Stony Brook University. It is a three-dimensional large-eddy model that can be run at both 2-D and 3-D situations under different resolutions, and it has been widely used in convection and cloud studies [*Fan et al.*, 2009; *Oreopoulos and Khairoutdinov*, 2003]. More detailed information about SAM is documented in *Khairoutdinov and Randall* [2003]. As in the standard GCSS setup, for BOMEX and ATEX, the LES simulation used horizontal resolution of 64 × 64 with 100 m grid spacing and vertical resolution of 75 levels from the surface to 3000 m. For ARM-SGP and RICO, the vertical resolution increases to 100 levels, reaching 4000 m at model top. Other configurations of the model, as well as the initial and forcing conditions, are identical to those recommended by the GCSS Working Group I intercomparison studies. Details of these experimental designs are documented in *Siebesma et al.* [2003] for BOMEX, *Vanzanten et al.* [2011] for RICO, *Stevens et al.* [2001] for ATEX, and *Brown et al.* [2002] for ARM-SGP. For all four cases, precipitation process is turned off so that total moisture is exactly conserved during model integration, which simplified the diagnosis. Diagnostic variables are calculated through the conditional sampling method every other minute.

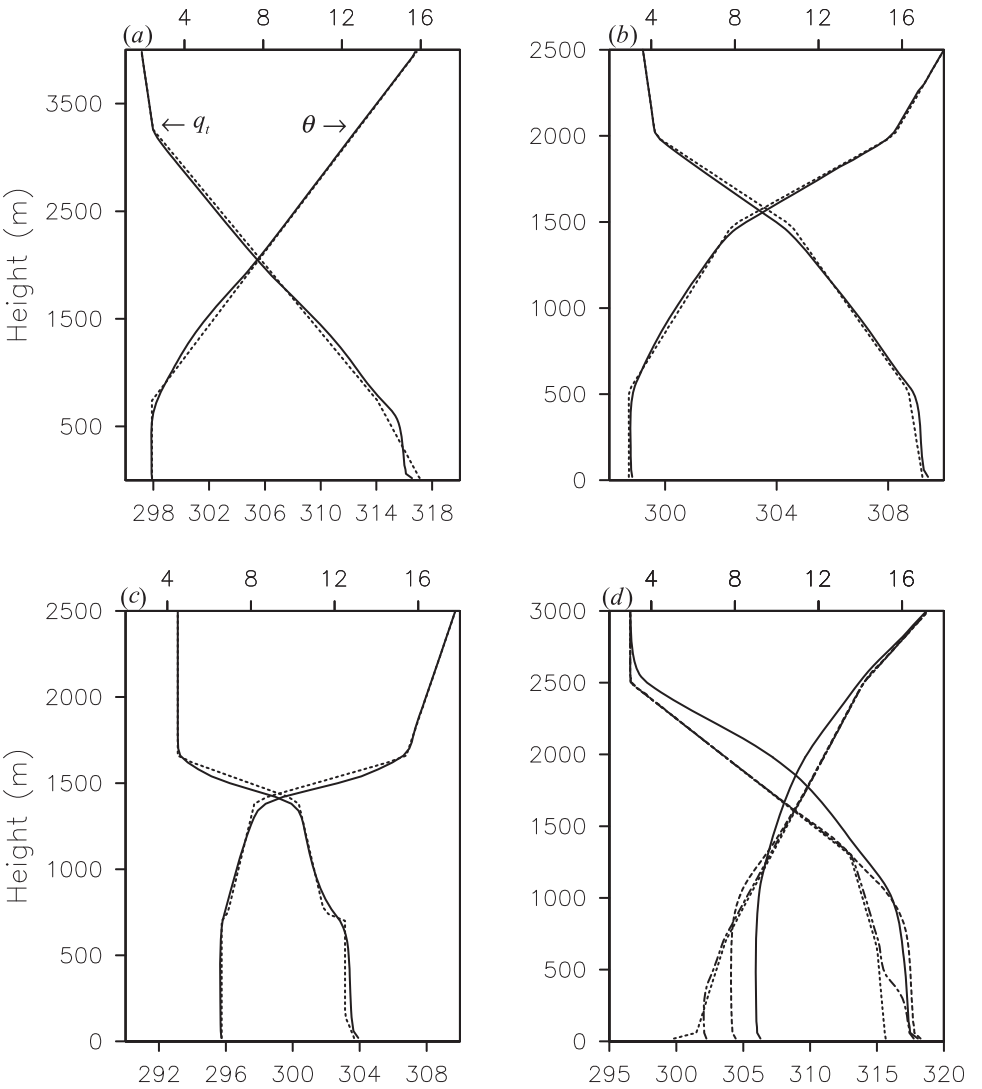

Figure 1. Initial (dotted line) and the last 4 h mean (solid line) profiles of θ and q_t for the case of (a) RICO, (b) BOMEX, and (c) ATEX. Instantaneous θ and q_t at time t = 0 h (dotted line), t = 3 h (dash-dotted line), t = 6 h (dashed line), and t = 9 h (solid line) for the case of (d) ARM-SGP (units: K for θ and g/kg for q_t).

2.3. LES Results

Figure 1 shows the initial (dotted line) and simulated vertical profiles of potential temperature θ and total water q_t. For the three maritime cases (Figures 1a–1c), all simulations achieved steady state. The last 4 h averages of the simulated θ and q_t are plotted (Figures 1a–1c, solid line). The main difference among these three cases lies in the inversion strength, increasing from RICO to BOMEX, to ATEX. For the nonsteady ARM-SGP case, the simulated θ and q_t at UTC 1130 (0530 local time), 1430, 1730, and 2030 are plotted in Figure 1d, which shows the development of the convective mixed layer during the day.

In order to diagnose the in-cloud properties from LES simulations, we used three sampling approaches: (1) the cloud core, defined as all the grid points that contain liquid water and have a positive vertical velocity and are positively buoyant, as used in *Siebesma and Cuijpers* [1995]; (2) cloud updraft, defined as all grid points that contain liquid water and upward motion, but positive buoyancy condition was not imposed, as used in *de Roode et al*. [2012]; (3) cloudy area, defined as grid points that contain liquid water.

Figures 2a–2d show the diagnosed cloud fraction a_c from the three types of plumes in the four cases, in which the dotted, dashed, and solid lines denote the core, updraft, and cloud plumes, respectively. The plume fraction has a maximum near the cloud bases (Figures 2a–2d), which suggests mixing of clouds with

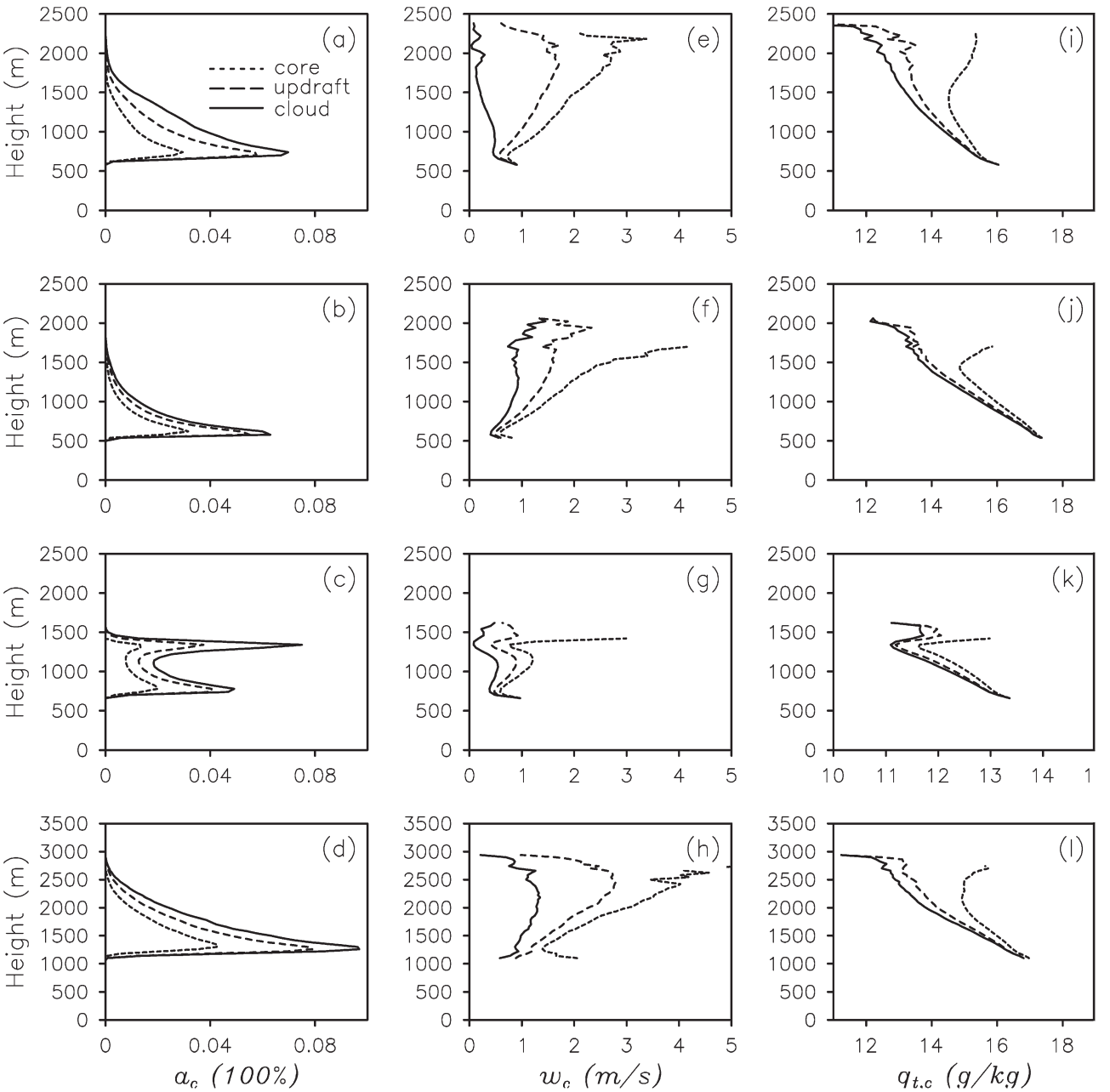

Figure 2. Profiles of cloud core ensemble averages of (a–d) updraft fraction a_c, (e–h) in-cloud vertical velocity w_c, and (i–l) total moisture $q_{t,c}$. From the top to bottom row, is for RICO, BOMEX, ATEX, and ARM-SGP at t = 10 h (15:30 local time), respectively. Dotted, dashed, and solid line stands for core, updraft, and cloud, respectively.

drier environmental air when the plume rises. There is a secondary peak in the ATEX case that corresponds to stratocumulus under a strong inversion. The plume fraction from the three definitions differs greatly. As expected, the area fraction of the core is about half of the cloud fraction. The area fraction of the updraft is in between, but it is closer to the cloud fraction than to the core fraction, indicating that the cloud area is mostly associated with upward motion, since downward motion tends to evaporate cloud droplets.

Figures 2e–2h show the mean vertical velocities w_c in the three types of plumes for the four cases. The mean vertical velocity w_c is in the range of about 0.5–5 m/s. The vertical velocity in the cloud core generally increases with height, consistent with the positive buoyancy. Its value in the cloud plume either decreases with height or increases with height at considerably small rate, with less than half of the cloud core velocity.

This is consistent with the larger fraction and entrainment of dry air shown in Figures 2a–2d. Again, the values for the updraft are in between those for the core and cloud plumes.

Figures 2i–2l show the mean total water $q_{t,c}$ in the three plume types for the four cases. The total water generally decreases with height up to the top of cloud, which is consistent with the mixing of cloudy air with environment air. Near the cloud top, the increase of total water with height in the core is related with the small number of sampling grid points as indicated by the small cloud amount. The decrease of total water with height in the updraft and in the cloud plumes is much larger than that of the core. Furthermore, the total water in the cloud area is close to that in the updraft, consistent with the inference made earlier that cloudy areas are mostly associated with upward motion.

These results point to the need to distinguish the three types of plumes in parameterizations of shallow convection, since they have very different properties. For radiative effects, cloud area is the most relevant definition; for condensation, cloud updraft may be more relevant, while for cloud nucleation, cloud core may be most important. In the following sections, we analyze the budget of vertical momentum for the three types of plumes and propose their parameterizations.

3. Entrainment Rate and In-Cloud Vertical Velocity Budget

The pioneer work of *Simpson and Wiggert* [1969] parameterizes w_c by the buoyancy forcing B_c and the drag term caused by entrainment rate ε (see equation (1)). Its physical basis is the vertical momentum equation integrated over a defined cloud area. In the present study, this equation is integrated in the three types of plumes—the core, the updraft, and the cloud grids defined in the previous section.

Following *Siebesma and Cuijpers* [1995], for an arbitrary variable χ, the expression for the entrainment rate ε can be written as follows:

$$\varepsilon(\chi_e-\chi_c)=\frac{\partial\chi_c}{\partial z}+\frac{1}{\rho w_c\sigma}\frac{\partial\overline{(\rho\sigma w''\chi'')_c}}{\partial z}+S_c, \tag{2}$$

where σ is the plume fraction; w is the vertical velocity; ρ is the air density; and S stands for sink and source terms. The subscripts "c" and "e" represent the mean value of the plume and the environment, respectively; the double prime represents derivation from the mean value within the plume; overbar stands for the average. This equation is written for the plume in the subgrid scale, under steady state assumption.

Equation (2) can be applied to the total water q_t and vertical velocity w. For the total water, when the top-hat approximation is used and precipitation process is switched off, the entrainment expression can be simplified as follows:

$$\varepsilon_{q_t}=\frac{-\frac{\partial q_{t,c}}{\partial z}}{q_{t,c}-q_{t,e}}. \tag{3}$$

For the vertical velocity, the entrainment rate can be derived from the following equation:

$$0=\left[-\frac{1}{2}\frac{\partial w_e}{\partial z}\right]+\left[-\frac{1}{\sigma\rho}\frac{\partial\overline{(\rho\sigma w''w'')_c}}{\partial z}\right]+\left[g\frac{T_{v,c}-T_{v,e}}{T_{v,e}}\right]+\left[-\frac{1}{\rho}\left(\frac{\partial p'}{\partial z}\right)_c\right]+[-\varepsilon_w w_c^2]. \tag{4}$$

The rhs terms of equation (4) are referred to as the advection, subplume turbulence (due to vertical change of the in-cloud vertical velocity variance), buoyancy forcing, pressure perturbation, and entrainment terms, respectively. These two equations have been widely used in previous studies [e.g., *Gregory*, 2001]. Approximations have to be made in obtaining (3) and (4) from the generic form of (1), including the lateral boundary condition of the plumes. Because of the impact of assumptions in arriving at equations (3) and (4), the two entrainment rates may not be exactly the same as well be shown next.

3.1. Entrainment Rate Diagnostics

The last 4 h mean entrainment rates calculated from the LES simulations by using equations (3) and (4) for the three maritime equilibrium cases and the 10th h for the ARM-SGP case are shown in Figure 3, with the

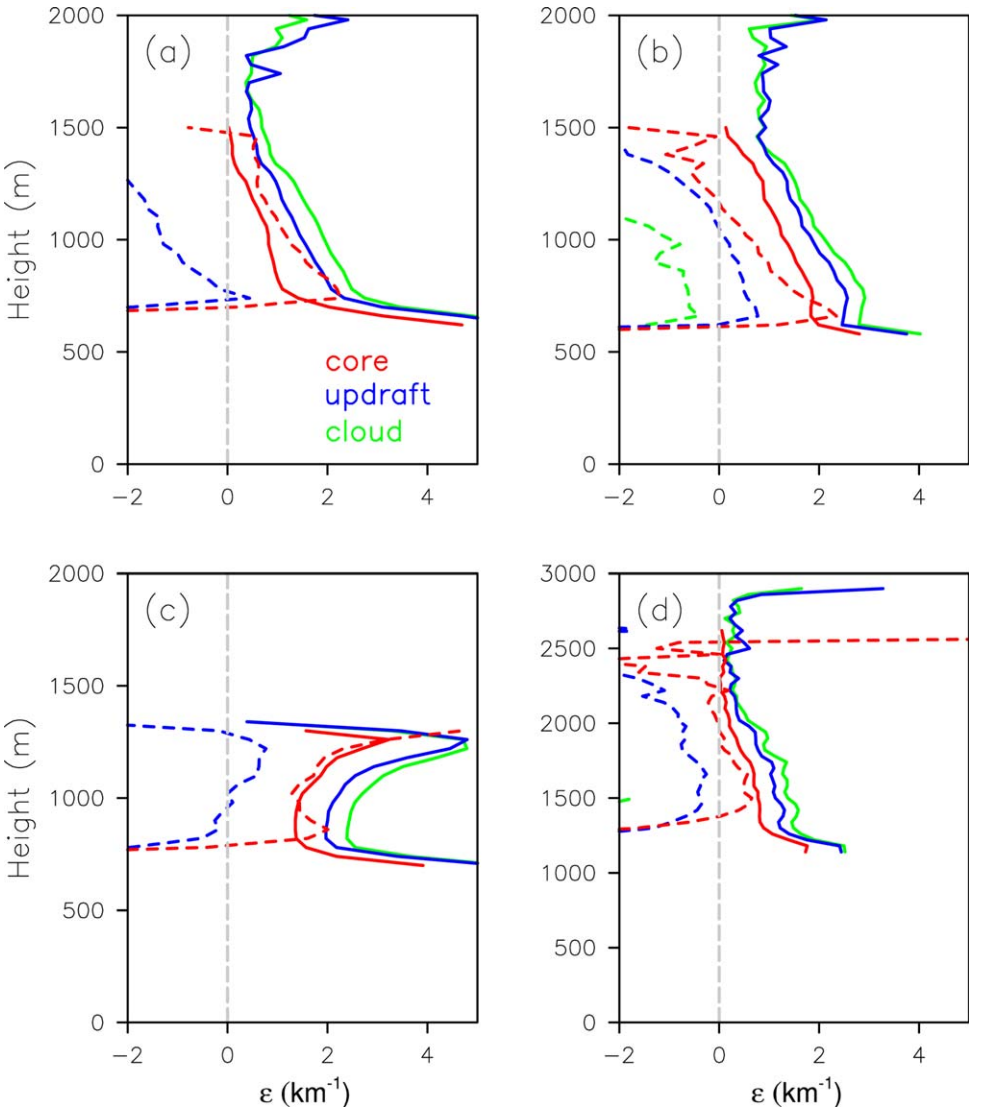

Figure 3. Entrainment rate diagnosed from equation (3) (solid line) and equation (4) (dotted line) for the case of (a) RICO, (b) BOMEX, (c) ATEX, and (d) ARM-SGP (units: km^{-1}). Red, blue, and green stands for core, updraft, and cloud, respectively.

red, blue, and green colors representing the core, updraft, and cloud plumes, respectively, and the solid line from equation (3), dashed line from equation (4). For the core plume, the entrainment rates from (3) and (4) exhibit similar profiles. Both decrease with height in the cases of BOMEX, RICO, and ARM. In the ATEX stratocumulus case, the two entrainment rates also show a similar profile, first decreasing and then increasing with height near cloud top. The larger entrainment rate near stratocumulus top in ATEX is indication of turbulent mixing caused by stratocumulus, consistent with the increasing cloud amount with height below the inversion. But a few differences can be noted between the two entrainment rates. ε_w is negative near cloud base. This is not physical. It is caused by the small sample of grid points in the calculation that has small vertical velocity near the cloud base. Because the negative values appear primarily at the cloud base, they do not have a significant impact on the momentum equation since the vertical velocity is small. In contrast to ε_w, ε_{q_t} has a large positive peak at the cloud base. Numerically, this large value is due to the relatively small difference of total cloud water across the cloud boundary that appears in the denominator of equation (3) and the diagnosed decrease of in-cloud total water with height shown in Figure 2. The diagnosed ε_{q_t} near the cloud base is therefore sensitive to small differences in the sampling method, which can affect the mass flux profile when used in plume models. This sensitivity however should not be a concern since the entrained mass flux near the cloud base has properties that are similar to the cloud base mass flux, which is

ultimately determined by a closure model. The overall agreement between ε_w and ε_{q_t} for the cloud core above cloud base is encouraging. It allows us to use one equation to calculate the other equation among (3) and (4).

For the updraft plume, however, significant difference is seen between the two entrainment rates in all cases between ε_w and ε_{q_t}. ε_{q_t} is positive and follows the ε_{q_t} in the core, but slightly larger than that in the core, indicating more entrainment for the updraft than for the core. ε_w (blue dashed line) is however considerably different from ε_{q_t} with values mostly negative. This negative value is consistent with *de Roode et al*. [2012] who also obtained negative entrainment rates. The ε_w is therefore not a true entrainment, but a parameter that includes both the true entrainment and the net effect of approximations in the vertical velocity equation (4). The negative values of ε_w indicates that the entrainment and lateral boundary forcing of the plume tend to accelerate the mean vertical velocity rather than decelerate it, which is likely due to dynamic forcing of the plume that is absent in the total water equation.

For the cloudy region (the green lines in Figure 3), the entrainment rate ε_{q_t} has the same shape as those for the core and updraft, but with larger values. It should be noted that the values of ε_w are so negative that they do not show up on the plot for Figures 3c and 3d. It is even more different from ε_w than the difference for the updraft. Therefore, for both the updraft and the cloud plume, the ε_w should not be interpreted as true entrainment. Instead, it should be considered as the net effect of entrainment and other approximations in equation (4). These approximations include the steady state assumption of the plume, and the assumption of $\chi_b = \chi_e$ for the entrained air which is satisfied only if convective clouds and the environmental air are both homogeneously distributed in their respective portions in a grid. In reality and in the LES simulations, a cloud plume may entrain air (χ_b) that was recently detrained from other clouds, which should be different to the average values within environment air (χ_e).

3.2. In-Cloud Vertical Momentum Budget

We show in Figure 4 the budget terms in equation (4) for all the four cases by using ε_w. For the core (Figures 4a–4d), the buoyancy term (orange solid) is positive at each level, due to the definition of the cloud core. The pressure perturbation term (green solid) is negative and it is the largest term in the upper cloud layer opposing the buoyancy forcing, with a magnitude generally larger than that of the buoyancy term near the cloud top. The advection term (purple solid) is mostly negative in the whole convective layers, but it is relatively small compared with other terms, which is in accordance with the increase of w_c with height (Figures 2e–2h). The subplume turbulence term (pink solid) is negative near the cloud base, near zero in the middle of clouds, and positive in upper levels in the three pure shallow convection cases (BOMEX, RICO, and ARM). These are consistent with increases of in-cloud vertical velocity variances from the cloud base and decreases of variances in the upper part of clouds. We note that the subplume acceleration to the mean vertical velocity is significant in the upper plume, comparable to the buoyancy term. For the ATEX stratocumulus case, the subplume turbulence term is negative, which is consistent with the upside-down convection originating from the top of stratocumulus clouds as reported before [e.g., *Randall*, 1984]. The entrainment terms (sienna solid), defined as $-\varepsilon_w w_c^2$, are generally negative above the cloud base but small in magnitude.

For the updraft plume, Figures 4e–4h show several notable differences from the budget in the core. First, the buoyancy term is much smaller. It becomes negative near the cloud top, consistent with the decrease of the vertical velocity in Figure 2. Second, the subgrid transport and the entrainment term become source terms of the vertical velocity except for the ATEX case in which the buoyancy term is still the dominant source. The pressure gradient force and the vertical transport terms are still sinks of vertical momentum. For the cloudy plume (Figures 4i–4l), the signs of the budget terms are generally similar to the updraft plume, except that the buoyancy term is even smaller.

4. Parameterization of In-Cloud Vertical Velocity

4.1. Determination of *b* (*a*=1)

We now evaluate the parameterization of the vertical velocity equation by using ε_{q_t} in equation (1) for the convective core. In a plume model, the buoyancy term is typically parameterized, but the pressure gradient term and the subplume transport are not easily available. One form of the vertical velocity parameterization is

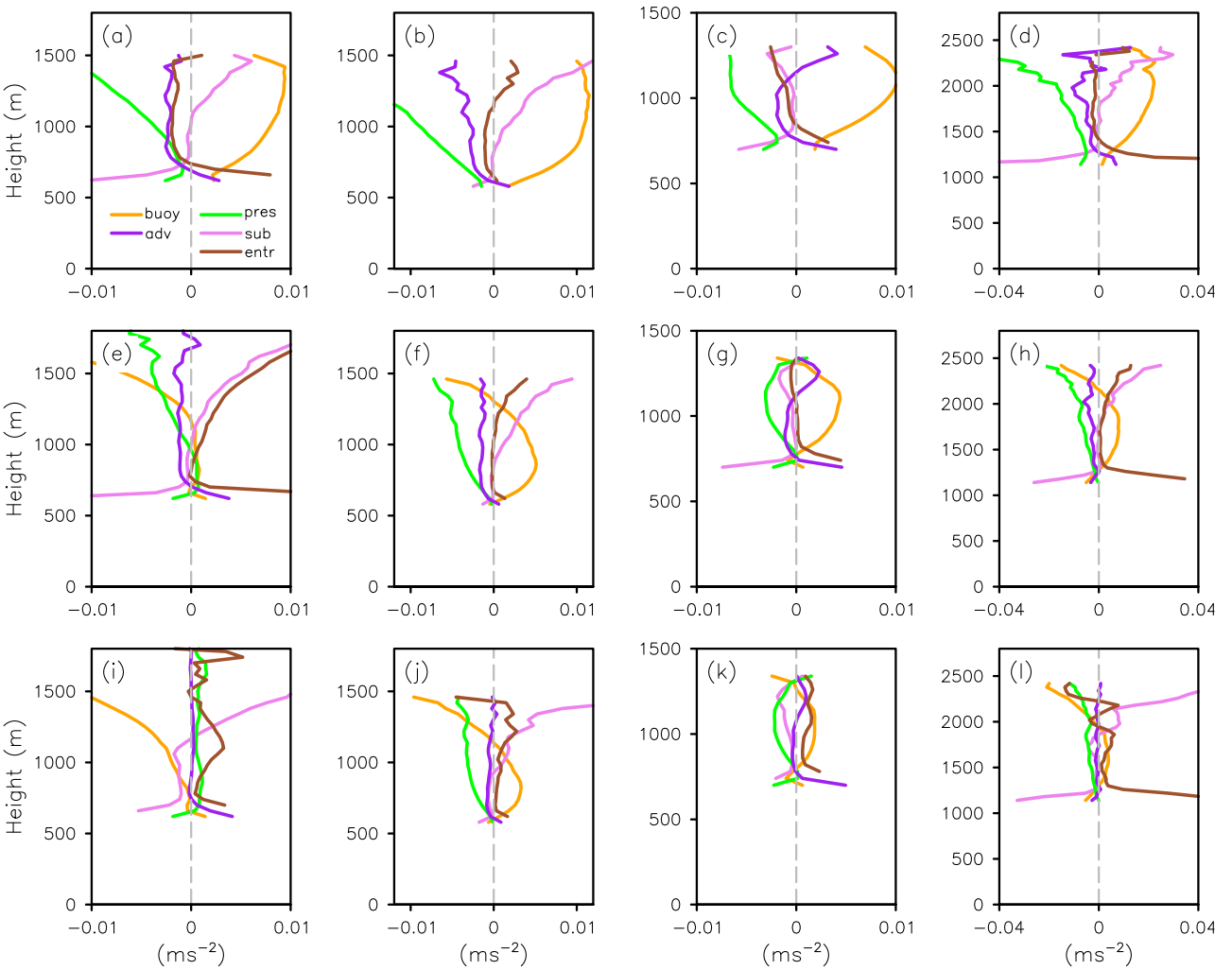

Figure 4. The last 4 h mean of in-cloud vertical moment budgets according to equation (4) for the case of (a, e, i) RICO, (b, f, j) BOMEX, (c, g, k) ATEX, and the 10th hourly mean for (d, h, l) ARM-SGP (units: ms^{-2}). Top, middle, and bottom stands for core, updraft, and cloud, respectively.

$$w_c \frac{\partial w_c}{\partial z} = B_c - b\varepsilon_{q_t} w_c^2, \tag{5}$$

where b is an empirical coefficient. In this formulation, the buoyancy term is kept intact ($a=1$) and the sum of the terms of subplume turbulence, pressure perturbation, and entrainment on the right-hand side of equation (4) is scaled with the entrainment term $-\varepsilon_{q_t} w_c^2$. Figure 5 shows the scatterplots of the sum of the three terms against the entrainment term for the core (Figure 5a), updraft (Figure 5b), and cloud plumes (Figure 5c) in the four cases. Each data point represents a 10 min averaged value at an arbitrary level within the plume. Overall, a positive correlation is indeed observed. However, there are considerable scatters in all cases, indicating that (5) has large uncertainties.

4.2. Determination of *a* (*b*=0)

The second form of the vertical velocity parameterization is

$$w_c \frac{\partial w_c}{\partial z} = B_c + \alpha B_c = a B_c. \tag{6}$$

The sum of the subplume turbulence, pressure perturbation, and entrainment in equation (4) is scaled with the buoyancy forcing. The scatterplots of the sum of the three terms versus the buoyancy forcing is

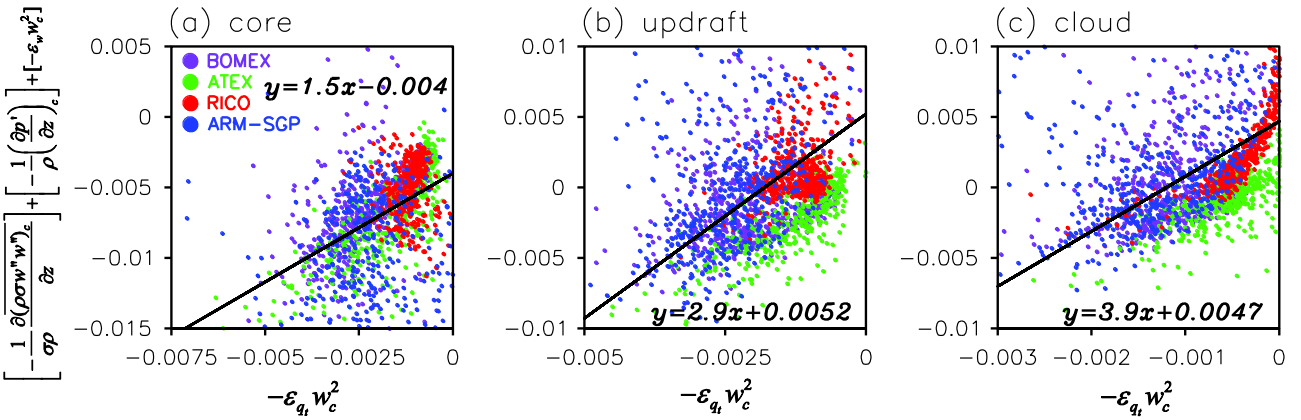

Figure 5. Scatterplots of the entrainment term (Abscissa) versus the residual term (Ordinate) for (a) core, (b) updraft, and (c) cloud (units: ms^{-2}).

displayed in Figure 6 for all the four cases. Overall, the points collapse reasonably well on a line, indicating the sum of the three terms can be reasonably represented by (6) by using the buoyancy term.

4.3. Determination of *a* and *b*

We now use the more generalized equation (1) to give the parameterizations for the three types of plumes. As in *de Roode et al.* [2012], we use the least error analysis to find better values of both *a* and *b* based on LES data points of each case by minimizing the cost function $f(a,b)$ written as follows:

$$f(a,b)=\sqrt{\frac{1}{N}\sum_{i=1}^{N}\left(aB_{c,i}-b\varepsilon_{q_t,i}w_{c,i}^2-w_{c,i}\frac{\partial w_{c,i}}{\partial z}\right)^2}, \tag{7}$$

where *N* stands for the number of LES data points. We derived the following three vertical velocity equations for the core, updraft, and cloud plumes, respectively:

$$w_c\frac{\partial w_c}{\partial z}=0.4B_c-1.06\varepsilon_{q_t}w_c^2, \tag{8}$$

$$w_c\frac{\partial w_c}{\partial z}=0.19B_c+0.29\varepsilon_{q_t}w_c^2, \tag{9}$$

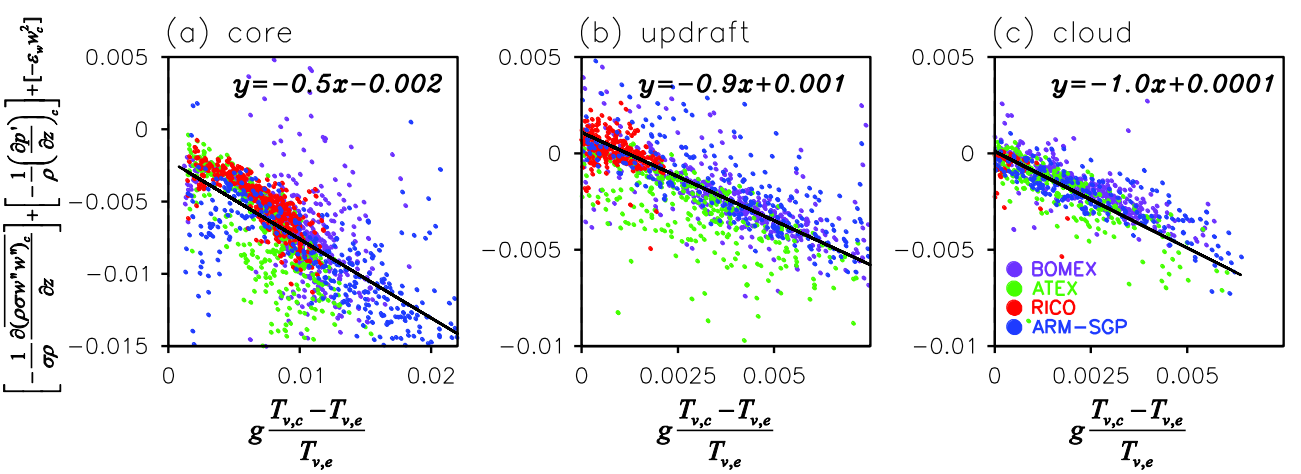

Figure 6. Same as Figure 5, except for scatterplots of the buoyancy forcing (Abscissa) versus the residual term (Ordinate) (units: ms^{-2}).

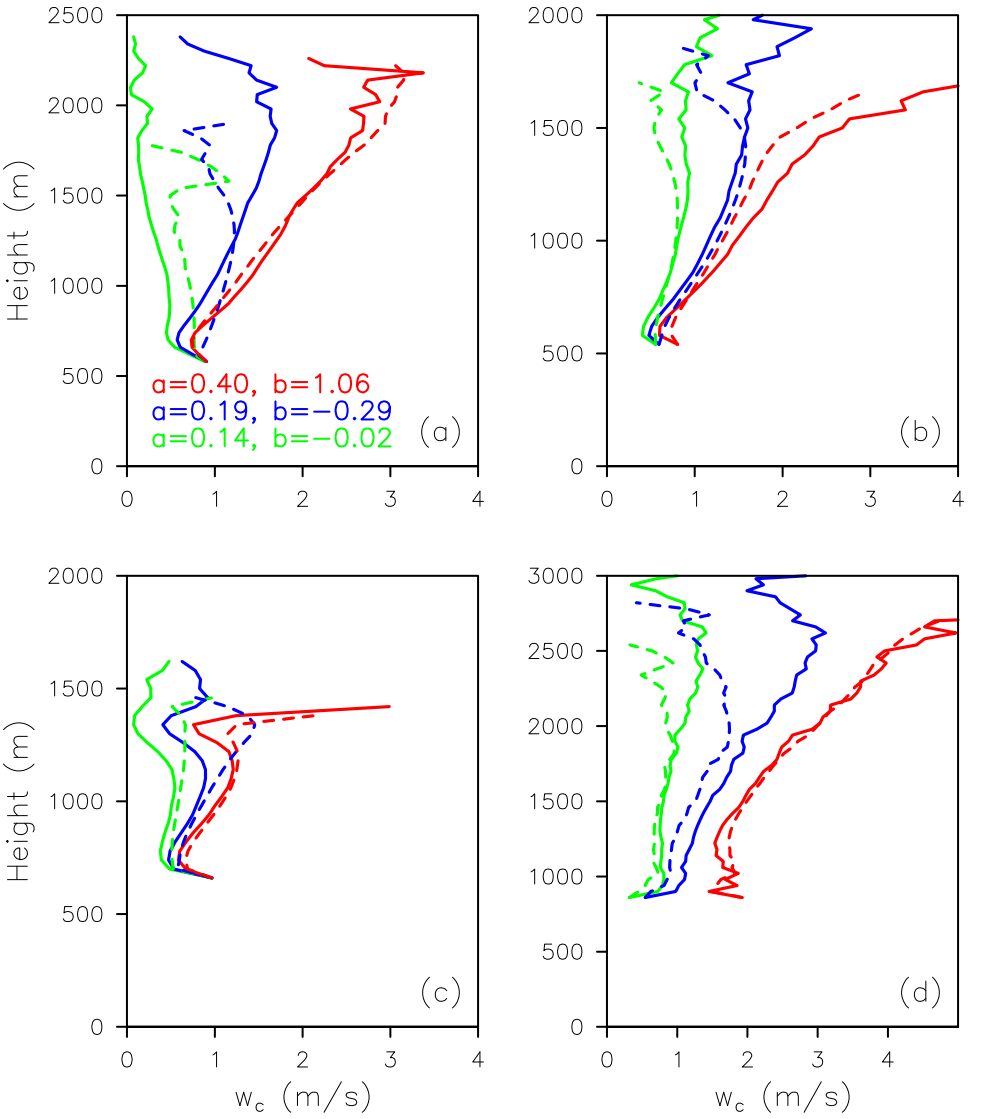

Figure 7. LES simulated (solid line) and reconstructed (dashed line) in-cloud vertical velocity w_c for the case of (a) RICO, (b) BOMEX, (c) ATEX, and (d) ARM-SGP (units: ms^{-1}). Red, blue, and green stands for core, updraft, and cloud, respectively.

$$w_c \frac{\partial w_c}{\partial z} = 0.14 B_c + 0.02 \varepsilon_{q_t} w_c^2. \tag{10}$$

It is noted that the entrainment term is positive for the updraft and for the cloud plumes. In a parameterization scheme, the buoyancy term is calculated based on the entrainment rate ε_{q_t}, which is parameterized separately but not covered in this paper.

To show the performance of the parameterization, the mean vertical velocity w_c for the three types of plumes is reconstructed according to equations (8–10) and compared with the directly sampled values by using the buoyancy B_c, entrainment rate ε_{q_t}, and w_c at cloud base. Figure 7 shows the LES simulated (solid line) and reconstructed (dashed line) w_c. For the convective core, the reconstructed w_c is very close to that of LES simulation, demonstrating equation (1) is well justified. For the updraft and cloud, the reconstructed w_c is generally close to that of LES simulation in the lower part, but with large biases in the upper level, which is presumably due to inconsistent ε_{q_t} and ε_w in the cloud updraft and cloud plumes.

The values of *a* and *b* used in the parameterizations in the literature are listed in Table 1. There are large differences, some of which are evidently due to the definition of the plumes. For example, *Soares et al.* [2004] used

a and *b* based on strong updrafts sampling, while *de Rooy and Siebesma* [2010] chose the cloud core sampling method. Therefore, when equation (1) is used, it is important to distinguish how the plume is defined.

Equations (8–10) by design are more accurate than the two alternate formulas of equation (5) in section 4.1 and equation (6) in section 4.2. Between the two simple alternate formulas of equations (5) and (6), the latter is more accurate according to Figures 5 and 6.

5. Conclusion

Four shallow cumulus case studies, including three equilibrium marine cases and one transient continent case, are simulated by using the SAM LES model to investigate the budget terms of plume vertical velocity for convective cores, updrafts, and clouds. For the cloud core, results show that the mean vertical velocity is primarily governed by acceleration of buoyancy forcing and subplume turbulence in the upper layer, and deceleration by the pressure gradient force and entrainment drag. The pressure perturbation and subplume turbulence are found to compensate each other significantly in the upper layer, leading to a small sum that is proportional to either buoyancy forcing or entrainment term, which forms the physical basis of the vertical velocity parameterization by using the buoyancy forcing and the entrainment drag. For the cloud updraft, the upward momentum source is significantly contributed by the subgrid transport and the entrainment term, particularly in the upper cloud layer. For the cloud plume, the buoyancy term is a momentum source only in the lower cloud layer. In the upper layer, the subgrid vertical transport is the dominant source.

The least error analysis is applied to obtain the optimal values for the scaling factors of *a* and *b* in the *Simpson and Wiggert* [1969] equation for each types of plumes. It is shown that the parameterization can accurately describe the vertical profiles of the mean plume velocity as long as the scaling coefficients are used differently for different types of plumes. These coefficients are given in the paper in equations (8–10) for convective core, convective updraft, and cloud plumes.

The present study does not discuss which sampling method is more preferable. The choice should depend on the purpose of the parameterizations. In current shallow convection parameterizations, only one type of plume is used, which is typically the cloud updraft. Our study showed that the entrainment rates calculated from the vertical momentum budget and total water budget in the cloud updrafts are very different. This is in contrast to cloud core for which the two entrainment rates are largely consistent. However, as long as the appropriate empirical coefficients are used, the plume vertical velocities can be derived with reasonable accuracy. Future parameterization of shallow convection may require the three types of plumes all parameterized separately to more accurately treat nucleation, condensation, and cloud area. Results in this paper can provide the basis for the vertical velocity calculations.

Acknowledgments
All LES data used in this study are available from the first author upon request. We thank the two anonymous reviewers whose comments have helped to improve the original paper. We also thank Marat Khairoutdinov for making his Large-Eddy Simulation model available to us. This research is supported by the Major National Basic Research Program of China (973 Program) on Global Change under Grant 2010CB951800, 973 program under Grant 2014CB441202, CAS Strategic Priority Research Program under Grant XDA11010402, and National Natural Science Foundation of China under Grant 41305102. Additional support was provided by the Biological and Environmental Research Division in the Office of Sciences of the US Department of Energy (DOE) and by NASA to the Stony Brook University.

References

Arakawa, A., and W. H. Schubert (1974), Interaction of a cumulus cloud ensemble with the large-scale environment, *Part I, J. Atmos. Sci.*, *31*(3), 674–701.

Bechtold, P., E. Bazile, F. Guichard, P. Mascart, and E. Richard (2001), A mass-flux convection scheme for regional and global models, *Q. J. R. Meteorol. Soc.*, *127*(573), 869–886.

Bretherton, C. S., J. R. McCaa, and H. Grenier (2004), A new parameterization for shallow cumulus convection and its application to marine subtropical cloud-topped boundary layers. Part I: Description and 1D results, *Mon. Weather Rev.*, *132*(4), 864–882.

Brown, A., R. Cederwall, A. Chlond, P. Duynkerke, J. C. Golaz, M. Khairoutdinov, D. Lewellen, A. Lock, M. MacVean, and C. H. Moeng (2002), Large-eddy simulation of the diurnal cycle of shallow cumulus convection over land, *Q. J. R. Meteorol. Soc.*, *128*(582), 1075–1093.

Cheinet, S. (2004), A multiple mass flux parameterization for the surface-generated convection. Part II: Cloudy cores, *J. Atmos. Sci.*, *61*(10), 1093–1113.

de Roode, S. R., A. P. Siebesma, H. J. Jonker, and Y. de Voogd (2012), Parameterization of the vertical velocity equation for shallow cumulus clouds, *Mon. Weather Rev.*, *140*(8), 2424–2436.

de Rooy, W. C., and A. P. Siebesma (2010), Analytical expressions for entrainment and detrainment in cumulus convection, *Q. J. R. Meteorol. Soc.*, *136*(650), 1216–1227.

Del Genio, A. D., and J. Wu (2010), The role of entrainment in the diurnal cycle of continental convection, *J. Clim.*, *23*(10), 2722–2738.

ECMWF (2010), IFS documentation—Cy36r1: Operational implementation 26 January 2010. Part IV: Physical processes, *European Centre for Medium-Range Weather Forecasts Tech. Rep.*, 171 pp, England. Available at http://old.ecmwf.int/research/ifsdocs/CY36r1/PHYSICS/IFSPart4.pdf.

Fan, J., T. Yuan, J. M. Comstock, S. Ghan, A. Khain, L. R. Leung, Z. Li, V. J. Martins, and M. Ovchinnikov (2009), Dominant role by vertical wind shear in regulating aerosol effects on deep convective clouds, *J. Geophys. Res.*, *114*, D22206, doi:10.1029/2009JD012352.

Fountoukis, C., A. Nenes, N. Meskhidze, R. Bahreini, W. C. Conant, H. Jonsson, S. Murphy, A. Sorooshian, V. Varutbangkul, and F. Brechtel (2007), Aerosol–cloud drop concentration closure for clouds sampled during the international consortium for atmospheric research on transport and transformation 2004 campaign, *J. Geophys. Res.*, *112*, D10S30, doi:10.1029/2006JD007272.

Gregory, D. (2001), Estimation of entrainment rate in simple models of convective clouds, *Q. J. R. Meteorol. Soc.*, *127*, 53–72.

Jakob, C., and A. P. Siebesma (2003), A new subcloud model for mass-flux convection schemes: Influence on triggering, updraft properties, and model climate, *Mon. Weather Rev.*, *131*(11), 2765–2778.

Khairoutdinov, M. F., and D. A. Randall (2003), Cloud resolving modeling of the ARM summer 1997 IOP: Model formulation, results, uncertainties, and sensitivities, *J. Atmos. Sci.*, *60*(4), 607–625.

Neggers, R. A., M. Köhler, and A. C. Beljaars (2009), A dual mass flux framework for boundary layer convection. Part I: Transport, *J. Atmos. Sci.*, *66*(6), 1465–1487.

Oreopoulos, L., and M. Khairoutdinov (2003), Overlap properties of clouds generated by a cloud-resolving model, *J. Geophys. Res.*, *108*(D15), 4479, doi:10.1029/2002JD003329.

Peng, Y., U. Lohmann, and R. Leaitch (2005), Importance of vertical velocity variations in the cloud droplet nucleation process of marine stratus clouds, *J. Geophys. Res.*, *110*, D21213, doi:10.1029/2004JD004922.

Pergaud, J., V. Masson, S. Malardel, and F. Couvreux (2009), A parameterization of dry thermals and shallow cumuli for mesoscale numerical weather prediction, *Boundary Layer Meteorol.*, *132*(1), 83–106.

Randall, D. A. (1984), Stratocumulus cloud deepening through entrainment, *Tellus, Ser. A*, *36*(5), 446–457.

Siebesma, A., and J. Cuijpers (1995), Evaluation of parametric assumptions for shallow cumulus convection, *J. Atmos. Sci.*, *52*, 650–666.

Siebesma, A. P., C. S. Bretherton, A. Brown, A. Chlond, J. Cuxart, P. G. Duynkerke, H. Jiang, M. Khairoutdinov, D. Lewellen, and C.-H. Moeng (2003), A large eddy simulation intercomparison study of shallow cumulus convection, *J. Atmos. Sci.*, *60*(10), 1201–1219.

Simpson, J., and V. Wiggert (1969), Models of precipitating cumulus towers, *Mon. Weather Rev.*, *97*(7), 471–489.

Soares, P., P. Miranda, A. Siebesma, and J. Teixeira (2004), An eddy-diffusivity/mass-flux parametrization for dry and shallow cumulus convection, *Q. J. R. Meteorol. Soc.*, *130*(604), 3365–3383.

Stevens, B., A. S. Ackerman, B. A. Albrecht, A. R. Brown, A. Chlond, J. Cuxart, P. G. Duynkerke, D. C. Lewellen, M. K. Macvean, and R. A. Neggers (2001), Simulations of trade wind cumuli under a strong inversion, *J. Atmos. Sci.*, *58*(14), 1870–1891.

Tiedtke, M. (1989), A comprehensive mass flux scheme for cumulus parameterization in large-scale models, *Mon. Weather Rev.*, *117*(8), 1779–1800.

Vanzanten, M. C., B. Stevens, L. Nuijens, A. P. Siebesma, A. Ackerman, F. Burnet, A. Cheng, F. Couvreux, H. Jiang, and M. Khairoutdinov (2011), Controls on precipitation and cloudiness in simulations of trade-wind cumulus as observed during RICO, *J. Adv. Model. Earth Syst.*, *3*, M06001, doi:10.1029/2011MS000056.

Wu, J., A. D. Del Genio, M. S. Yao, and A. B. Wolf (2009), WRF and GISS SCM simulations of convective updraft properties during TWP-ICE, *J. Geophys. Res.*, *114*, D04206, doi:10.1029/2008JD010851.

Wyant, M. C., C. S. Bretherton, H. A. Rand, and D. E. Stevens (1997), Numerical simulations and a conceptual model of the stratocumulus to trade cumulus transition, *J. Atmos. Sci.*, *54*(1), 168–192.

Zhang, G. J., and N. A. McFarlane (1995), Sensitivity of climate simulations to the parameterization of cumulus convection in the Canadian Climate Centre general circulation model, *Atmos. Ocean*, *33*(3), 407–446.